Nanotechnology **19** (2008) 035203 (7pp) doi:10.1088/0957-4484/19/03/035203

Organic memory using [6,6]-phenyl-C_{61} butyric acid methyl ester: morphology, thickness and concentration dependence studies

Jayanta K Baral[1,2,6], Himadri S Majumdar[1], Ari Laiho[3], Hua Jiang[4,5], Esko I Kauppinen[4,5], Robin H A Ras[3], Janne Ruokolainen[3], Olli Ikkala[3] and Ronald Österbacka[1,6]

[1] Center for Functional Materials and Department of Physics, Åbo Akademi University, Porthansgatan 3, Turku, FIN-20500, Finland
[2] Graduate School of Materials Research, Universities of Turku, Turku, Finland
[3] Department of Engineering Physics and Mathematics, and Center for New Materials, Helsinki University of Technology, Nanopoli, PO Box 5100, FIN-02015 HUT, Finland
[4] NanoMaterials Group, Laboratory of Physics and Center for New Materials, Helsinki University of Technology, PO Box 5100, FIN-02015 TKK, Finland
[5] VTT Biotechnology, PO Box 1000, FIN-02044 VTT, Finland

E-mail: jayanta.baral@abo.fi and ronald.osterbacka@abo.fi

Received 23 August 2007, in final form 15 November 2007
Published 13 December 2007
Online at stacks.iop.org/Nano/19/035203

Abstract

We report a simple memory device in which the fullerene-derivative [6,6]-phenyl-C_{61} butyric acid methyl ester (PCBM) mixed with inert polystyrene (PS) matrix is sandwiched between two aluminum (Al) electrodes. Transmission electron microscopy (TEM) images of PCBM:PS films showed well controlled morphology without forming any aggregates at low weight percentages (<10 wt%) of PCBM in PS. Energy dispersive x-ray spectroscopy (EDX) analysis of the device cross-sections indicated that the thermal evaporation of the Al electrodes did not lead to the inclusion of Al metal nanoparticles into the active PCBM:PS film. Above a threshold voltage of <3 V, independent of thickness, a consistent negative differential resistance (NDR) is observed in devices in the thickness range from 200 to 350 nm made from solutions with 4–10 wt% of PCBM in PS. We found that the threshold voltage (V_{th}) for switching from the high-impedance state to the low-impedance state, the voltage at maximum current density (V_{max}) and the voltage at minimum current density (V_{min}) in the NDR regime are constant within this thickness range. The current density ratio at V_{max} and V_{min} is more than or equal to 10, increasing with thickness. Furthermore, the current density is exponentially dependent on the longest tunneling jump between two PCBM molecules, suggesting a tunneling mechanism between individual PCBM molecules. This is further supported with temperature independent NDR down to 240 K.

(Some figures in this article are in colour only in the electronic version)

1. Introduction

Over the last decade, enormous strides have been made in the field of organic electronics. One of the emerging research areas in this field is nonvolatile memory cells. Since the beginning of the 21st century, research and development on first-generation organic memories have been carried out by the various research groups worldwide [1–7]. In one of our previous communications [6] we discussed a simple single layer sandwich structure memory device based on a C60 fullerene mixed with an insulating polystyrene polymer matrix concurrently with and independent of Paul *et al* [7]. The

[6] Authors to whom any correspondence should be addressed.

device showed bistability (i.e. two distinct conducting states) and negative differential resistance (NDR) in current density–voltage (J–V) characteristics. The effect of bistability can be very promising for memory devices, especially when nonlinear device characteristics can be combined with large off-currents [8]. The second effect, namely negative differential resistance (NDR), is a robust phenomenon that is possibly suitable for small-scale memories to be produced with mass-fabrication techniques such as printing techniques, since it is not so sensitive to variations in the processing, as will be shown. Even though the devices do not exhibit large ON/OFF ratios (defined as the difference between the high- and low-impedance states at a given read voltage) the effect is easy to control under rugged printing conditions. The devices showing the NDR phenomenon can be used as a memory element, as has been reported earlier [9]. The detailed circuit design for the above-mentioned memory system by using NDR-type devices is available in the reference and is beyond the scope of this paper.

The previously observed bistability and NDR in various films have been explained by various mechanisms such as filamentary conduction [10], electroforming [11], Coulomb blockade [12], highly correlated electron effects [13], electrochemical doping [14] and electric-field-induced charge transfer [15]. In this paper we report a fullerene-derivative PCBM based memory device which showed stable NDR in the sample thickness range between 200 and 350 nm. We found that the threshold voltage is insensitive to the device thickness. The ON/OFF ratio in the NDR regime is stable and larger than 10, which is promising from a memory application point of view. We discuss the origin of the NDR in these devices as due to tunneling between individual PCBM molecules.

2. Fabrication and experimental details

Our device architecture is sandwich type, in which Al/PS:PCBM/Al thin films were fabricated on thoroughly cleaned glass substrates. Chemical compounds such as polystyrene (PS), polyphenylene oxide (PPO), also known as polyphenylene ether (PPE), and chloroform ($CHCl_3$), from Sigma-Aldrich, and [6,6]-phenyl-C61 butyric acid methyl ester (PCBM), from Nano-C Inc., were used as received. Parent solutions of PCBM in chloroform (concentration 10 mg ml^{-1}) and PS in chloroform (concentration 50 mg ml^{-1}) were used to prepare the PCBM:PS nanocomposite. PCBM:PS films were spin-coated on ∼30–35 nm Al-coated glass substrates. The films were then annealed at 80 °C for 90 min under a vacuum of $\sim 1 \times 10^{-3}$ mbar. The device was finally completed by evaporating a ∼30–35 nm Al electrode on top of the PCBM:PS thin films. Both the top and bottom Al electrodes were evaporated at a pressure of $\sim 1 \times 10^{-6}$ mbar with a uniform rate of evaporation 1.0–1.2 Å s^{-1} to avoid Al penetration into the active medium. The thicknesses of thermally evaporated metal electrodes were measured by a MAXTEK, Inc. Thickness Monitor TM-100. The thickness of the films was determined with a Park Scientific Instruments AUTOPROBE *cp* atomic force microscope and charge extraction in a linearly increasing voltage (CELIV) technique; a detailed description of using CELIV for the thickness determination is given in [16]. The active area of the devices was 2×2 mm^2. Electrical characterization of the devices was performed by using a Keithley 2400 programmable voltage source meter and a Keithley 617 programmable electrometer or an Agilent 4142B Modular DC source/monitor. All device fabrication and electrical characterization was carried out inside a nitrogen filled glove box. Similar electrical properties were observed upon changing the polarity between the top and bottom electrodes.

Structural characterization was done with transmission electron microscopy (TEM) on devices prepared onto NaCl substrates (Sigma-Aldrich, IR crystal window). For plan-view TEM the devices were floated off from the substrate onto de-ionized water and collected onto copper TEM grids. For cross-sectional TEM a small droplet of epoxy was first put on top of the sandwiched device and cured at room temperature. The epoxy/device structure was peeled off from the NaCl substrate by dissolving the substrate in de-ionized water. Finally the epoxy/device structure was covered with an embedding epoxy, and after curing at room temperature, thin sections (70 nm thick) from the epoxy/device/epoxy structure were sectioned with an ultra-microtome and collected onto copper TEM grids. Bright-field TEM was performed on an FEI Tecnai 12 transmission electron microscope with a LaB_6 filament operating at an accelerating voltage of 120 kV. A more quantitative analysis of the device cross-sections was done using a high-resolution field emission transmission electron microscope (FE-TEM, Philips CM-200 FEG-(S)TEM-Super Twin) equipped with an energy dispersive x-ray spectroscopy (EDX) analyzer (Noran Voyager M3305).

Transmittance (T) and reflectance (R) of the thin films spin-coated on quartz substrates were measured with a Perkin-Elmer Lambda 950 spectrophotometer equipped with an integrating sphere (Labsphere). Optical densities (ODs) of the thin films were further determined from these values according to $\mathrm{OD} = -\log_{10}(\frac{T}{1-R})$. The absorption coefficient α is related to the optical density by $\alpha = \frac{\mathrm{OD} \ln 10}{L}$, where L is the film thickness that was determined with a DEKTAK 3 surface profiler.

3. Results and discussion

In figure 1(a) the typical current density–voltage (J–V) characteristics of an Al/PCBM:PS/Al device are shown. The devices are scanned through the voltage sequence 0 to +8 V, +8 to −8 V in steps of 0.5 V. At low voltages (less than 2 V) the pristine device exhibits low conductivity; repeated scans below 2 V do not alter the impedance state of the device. When the bias reaches approximately 3 V, the device makes an abrupt transition from the high-impedance (OFF) state to the low-impedance (ON) state and stays there for all measurements thereafter. We note that this device behavior is similar to what is physically observed in tunnel diodes. The voltage for this transition is denoted the threshold voltage (V_{th}). The J–V curves are 'N-shaped', i.e. the current decreases with increasing voltage, having a local current maximum at V_{max} and a local current minimum at V_{min}. This is called an N-type NDR [6].

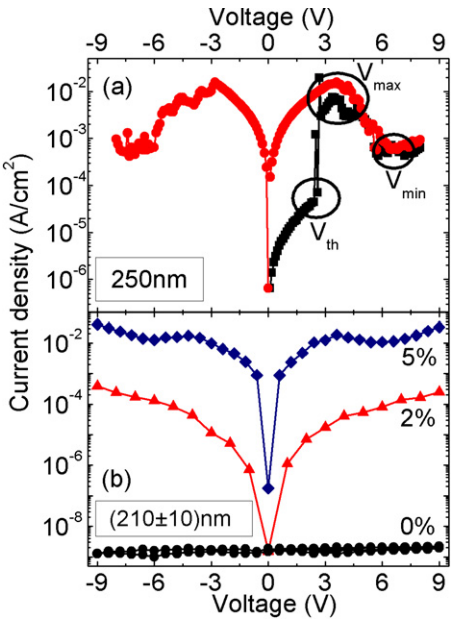

Figure 1. (a) Absolute value of current density (J) as a function of voltage (V) for a 250 nm thick 5 wt% Al/PCBM:PS/Al device. Squares (■) show the first bias scan direction of the devices from 0 to +8 V and then the circles (●) show the scan directions later on from +8 V to −8 V. The threshold voltage (V_{th}), maximum voltage (V_{max}) and minimum voltage (V_{min}) are circled. In (b), the J–V plot shows the absolute value of current density as a function of voltage for 0 wt% PCBM:PS (circles: ●), 2 wt% PCBM:PS (triangles: ▲) and 5 wt% PCBM:PS (squares: ■) devices of 210 ± 10 nm thickness, showing the appearance of NDR above 4 wt%.

It has been reported recently [1, 10] that the electrodes play a crucial role for obtaining switching behavior, whereas the organic material between the electrodes has only minor influence in their device behavior. Filamentary conduction due to electroforming at one of the Al electrodes is attributed as another cause for the switching effect observed in Al/PS/Al devices [17]. To check whether the NDR behavior in our Al/PCBM:PS/Al devices is caused by electroforming we have carefully performed the following experiments. Three similar devices from separate solutions with 0 wt% of PCBM in PS (termed as a PS-only device), 2 wt% of PCBM in PS (termed as a 2 wt% PCBM device) and 5 wt% of PCBM in PS (termed as a 5 wt% PCBM device) were fabricated with the same Al/PCBM:PS/Al structure of 210 ± 10 nm thickness, and the results are shown in figure 1(b). We observed that the current density values for devices made from 0 wt% (PS-only) solution are orders of magnitude smaller than for the devices from 2 to 5 wt% solution, suggesting that the device works like an insulator in the absence of PCBM in the film. By merely adding a small amount of PCBM to the PS (i.e. from 0 to 2 wt%), a different device characteristic is observed with comparatively larger current density values than in the PS-only device, but no NDR was observed. Upon further increasing the amount of PCBM molecules with respect to PS (i.e. above 4 wt%), NDR is consistently observed.

In order to further clarify the chances of Al penetration into the active intermediate PCBM:PS layer, we have also done TEM studies on both pristine and used Al/PCBM:PS/Al devices. In figures 2(a) and (b) we show a plan-view and a cross-sectional TEM image, respectively, of a used device made from a solution of 5 wt% PCBM in PS. The ripples in the cross-sectional image are due to the cutting procedure that was done at a 45° angle with respect to the electrodes. The plan-view image was taken next to a film edge from as thin a region as possible to observe the smallest particles possible. One should note that the very small structuring (<1 nm) visible in the plan-view image is a TEM artifact that is also known as a 'salt and pepper' structure [18]. The images show neither penetration of Al into the active medium from the evaporated top electrode nor the formation of PCBM aggregates inside the PCBM/PS films, and in addition the PCBM molecules seem to be homogeneously dispersed in

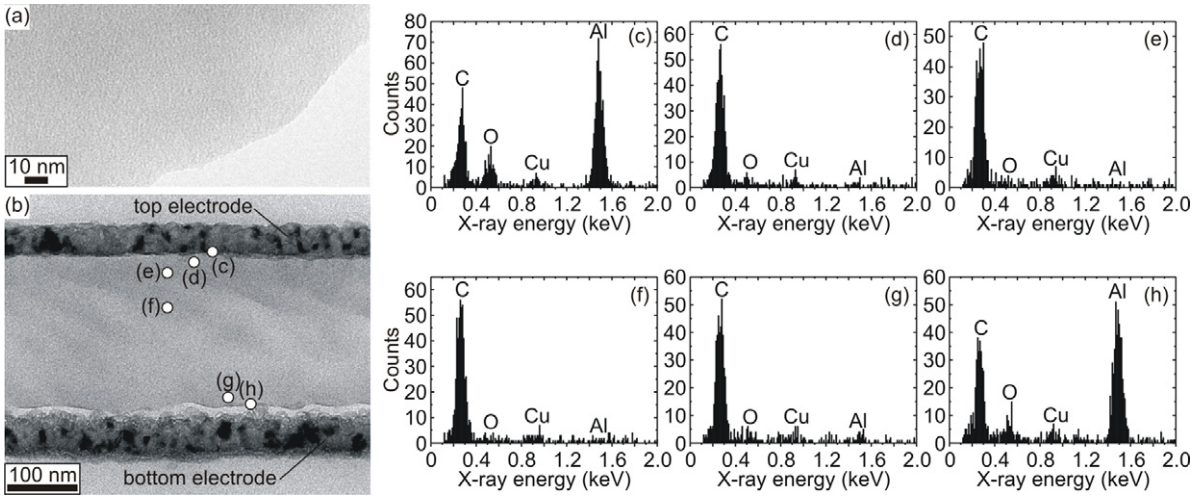

Figure 2. (a) Plan-view TEM image of a used 5 wt% PCBM:PS device close to an edge (the thin film is on the left-hand side of the image). (b) Cross-sectional TEM image of the same device consisting of a 250 nm thick 5 wt% PCBM:PS film sandwiched between the top and bottom Al electrodes. The points for the quantitative EDX elemental analysis are indicated as circles in the cross-section and the corresponding results from the EDX analysis are shown in (c)–(h). The appearance of copper (Cu) in the spectra is due to the background from the copper TEM grids.

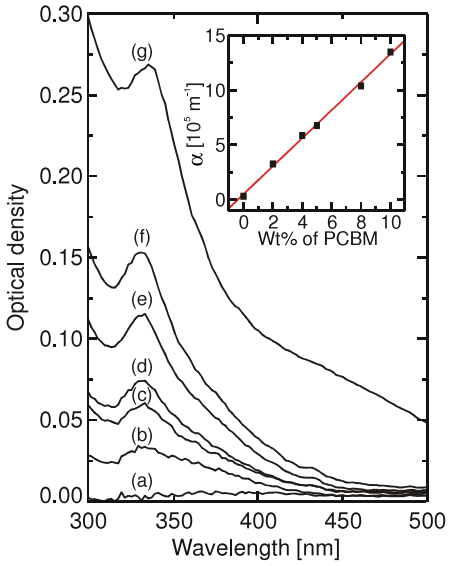

Figure 3. Optical absorption spectra of spin-coated thin films of (a) pure PS ($L = 244$ nm), (b) 2 wt% PCBM/PS ($L = 236$ nm), (c) 4 wt% PCBM/PS ($L = 238$ nm), (d) 5 wt% PCBM/PS ($L = 253$ nm), (e) 8 wt% PCBM/PS ($L = 256$ nm), (f) 10 wt% PCBM/PS ($L = 261$ nm) and (g) pure PCBM ($L = 356$ nm). The inset shows the absorption coefficients α for each thin film at a wavelength of 334 nm.

the PS matrix. To further quantify the absence of Al in the PCBM/PS layer we performed EDX from the points marked in the device cross-section (figure 2(b)). The corresponding spectra obtained from these points (figures 2(c)–(h)) show an abrupt disappearance of Al as one goes from the top Al/PCBM:PS interface (figure 2(c)) into the active PCBM:PS layer (figures 2(d)–(f)). In other words, the spectra verify that the slow evaporation rate of Al (1.0–1.2 Å s^{-1}) does not lead to penetration of Al into the active PCBM:PS layer. From the above observations we conclude that the observed consistent NDR in our Al/PCBM:PS/Al devices cannot be due to the deliberate or unintentional inclusion of metal nanoparticles from the thermal evaporation of the top Al electrode, but due to PCBM molecules in the PS matrix.

To further prove the presence of the PCBM molecules in the thin films, we measured the optical absorption spectra of different films. The optical densities of thin films of PS, 2 wt% PCBM/PS, 4 wt% PCBM/PS, 5 wt% PCBM/PS, 8 wt% PCBM/PS, 10 wt% PCBM/PS and pure PCBM are shown in figure 3. The peak around $\lambda = 334$ nm is attributed to PCBM absorption and the optical densities at this particular wavelength together with film thicknesses L were used to determine the absorption coefficients of each composition at 334 nm. If we assume that the densities of PCBM ($\rho_{PCBM} = 1500$ kg m^{-3}) [19], PS ($\rho_{PS} = 1060$ kg m^{-3}, Sigma-Aldrich) and the composite (ρ_C) are comparable and that the components of the composite are non-interacting, the overall absorption coefficient of the composite is given by Savenije *et al* [20] as $\alpha = \alpha_{PS} + wt_{PCBM}(\alpha_{PCBM} - \alpha_{PS})$, where wt_{PCBM} is the weight fraction of PCBM. The good linear dependence of α on wt_{PCBM} shown in the inset of figure 3 not only proves the existence of PCBM in the thin films but also shows that the amount of PCBM with respect to PS behaves in the same fashion between solutions and thin films prepared from these solutions.

Cölle *et al* [10] have argued that in filamentary conditions the space charge limited conduction (SCLC) currents are orders of magnitude lower than the 'ON' state current. To clarify this in the case of our devices we have calculated the SCLC current in the (only) PCBM devices, considering the mobility $\mu = 10^{-3}$ cm^2 V^{-1} s^{-1}. We found that the current densities in our PCBM:PS films are two orders of magnitude lower in the ON state than the calculated (trap free) SCLC current. Filamentary conduction has been shown to be a general observation in disordered systems [21]. The current filaments in thin films grow according to a well-known mechanism called 'electrical-treeing' [22]. These filaments could cause irreversible changes in the local structure due to the low glass transition temperature ($T_g \approx 100\,^{\circ}C$ for PS) of PS insulating polymer. However, the glass transition temperature of the insulating polymer matrix can be increased by introducing another polymer matrix material, namely polyphenylene ether (PPE), that is perfectly miscible in PS but has a significantly higher glass transition temperature, $T_g > 200\,^{\circ}C$. Devices having PPE or PS/PPE as the polymer matrix show exactly similar device characteristics without a change in the threshold voltage. This is evidence against irreversible changes in the devices.

So far we have emphasized the fact that electroforming is not the working principle in our devices. We will now put forward what we think are the probable mechanisms for the switching and NDR observed in our devices. One probable explanation can be multiple tunneling and the Coulomb blockade effect [12]. Coulomb blockade is a purely quantum mechanical phenomenon and NDR and Coulomb staircases observed in single- to four-molecule systems cannot be simplified for our devices. The NDR phenomenon observed in the PCBM:PS devices is more electronic in nature. It has previously been shown that the change of conductivity in a nanocomposite system can be attributed to dipolar carrier trapping [23], where injected electrons and holes are trapped in the conduction and valence bands of the nanoclusters, respectively. This contributes to the increase of conductivity at V_{th}. This can also be due to initial electronic charging of the PCBM nanoclusters and subsequent emission of electrons and tunneling at higher fields [24]. Rozenberg *et al* [25] have put forward a phenomenological model also based on tunneling between metal nanoclusters embedded in an insulating matrix that gave rise to switching. However, the physical reason for the NDR is still not very explicit. The PCBM nanoclusters embedded in the PS matrix can be visualized as chargeable particles separated by a tunneling barrier of PS. Deformation of the tunneling barrier height and width at higher electric field give rise to the non-linear current–voltage characteristics.

NDR was observed consistently in all PCBM:PS devices made from solutions with concentration varying between 4 and 10 wt%. It was also very consistent within the thickness range of 200–350 nm for all the concentrations. Beyond this concentration and thickness range the NDR ceases to exist. In figure 4, we show the V_{th}, V_{max} and V_{min} in the NDR regime of the measured 5 wt% Al/PCBM:PS/Al devices as a

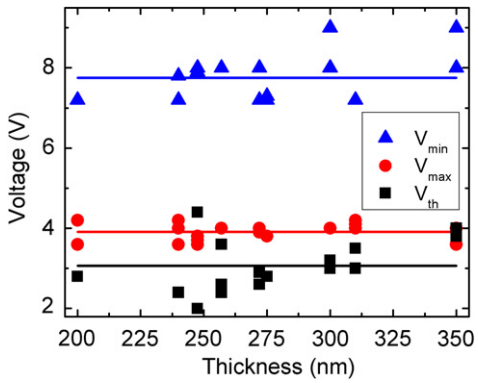

Figure 4. Voltage (V) as a function of thickness (L) showing the threshold voltage (V_{th}), maximum voltage (V_{max}) and minimum voltage (V_{min}) denoted by the squares (■), circles (●) and triangles (▲) respectively in the negative differential resistance regime. The points show the maximum deviation taken from a set of at least five structures each.

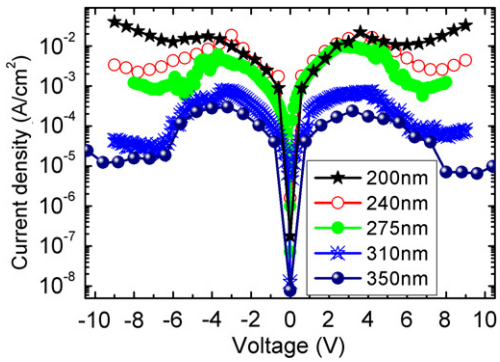

Figure 5. Absolute value of current density as a function of voltage of a 5 wt% device at different thickness (200–350 nm). The ratio of V_{max} to V_{min} decreases on decreasing the inter-electrode distance with increase in the ON state current density of the NDR regime.

function of thickness of the PCBM:PS layer. This indicates that the transport property of the PCBM:PS devices greatly hindered by excessive thickness of the nanocomposite, and insufficient PCBM concentration in it. Figure 4 also shows that the parameters V_{th}, V_{max} and V_{min} vary only within a small voltage range for all thicknesses, making these devices suitable for application in large-scale manufacturing processes, such as printing. In our previous communication [6], we have already shown how NDR can be used for multilevel switching. Also, the current ratio for V_{max} and V_{min} in the NDR regime is more than or equal to 10, which is comparable to the performance of Esaki or tunnel diodes in terms of application.

The variation of current density of a 5 wt% PCBM:PS device for different film thickness is plotted separately in figure 5. The current density increases as the thickness of the PCBM:PS devices decrease. Physically, an increase in the PCBM:PS layer thickness indicates an increase in number of tunneling barriers between the two Al electrodes. This, in turn, will decrease the probability of the injected electrons to reach the counter-electrode, effectively reducing the device current density. The current density ratio between V_{max} and V_{min} in the

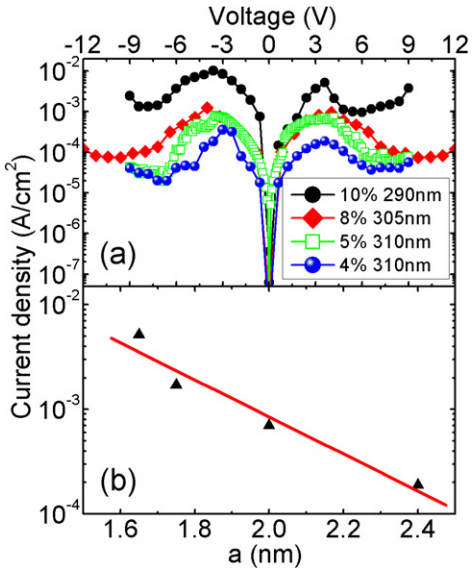

Figure 6. (a) Absolute value of current density as a function of voltage for different PCBM concentrations (4, 5, 8 and 10 wt%) keeping the device thickness at $L = (300 \pm 10)$ nm. (b) The absolute value of maximum current density (J_{max}) as a function of calculated average inter-molecular distance (a) between the centers of two PCBM molecules, showing that the exponential current increases with increase in PCBM concentration.

NDR regime decreases from 40 to 2 with decreasing thickness. The reduction of current suggests the possibility of another switching mechanism in very thin films [10].

In another experiment we kept the thickness of the active PCBM:PS layer constant while varying the PCBM concentration in the devices. We fabricated devices of thickness 300 ± 10 nm from 4, 5, 8 and 10 wt% PCBM:PS solutions. The current density increases as the concentration of the PCBM in PS increases, as shown in figure 6(a). Since we can safely assume that the PCBM molecules are homogeneously spread inside the film based on the TEM images, we can calculate the average inter-molecular distance a from center to center of two PCBM molecules using volume concentration and geometrical considerations. Let us consider a tunneling rate proportional to $\exp(-2\gamma r)$, where 2γ is the wavefunction overlap factor and r is the distance between hopping sites. In figure 6(b) we plot the ON-state current density at V_{max} in our devices as a function of the calculated average inter-molecular distance a, and the line is a fit to $J \propto \exp(-\frac{a}{r_0})$, with the constant r_0 is being equal to 3.5 nm.

For a positionally disordered hopping system, the mobility will be proportional to the rate of the longest jump [26, 27] needed to get a percolative network. Following a similar argument we suggest that the current density in these films will be proportional to the longest tunneling rate. It has been shown that the longest hopping distance r_{max} for a positionally disordered hopping system scales with the average inter-site hopping distance as $r_{max} = \lambda a$, where λ is a numerical factor, being 1.39 for a 3D positionally disordered system [26, 27]. Using this in the usual tunneling formula $\mu \propto \exp(-2\gamma r_{max})$, we obtain $2\gamma\lambda a = \frac{a}{r_0}$, $=> \gamma = \frac{1}{2\lambda r_0} \cong 1$ Å^{-1}, indicating that the tunneling sites are well localized.

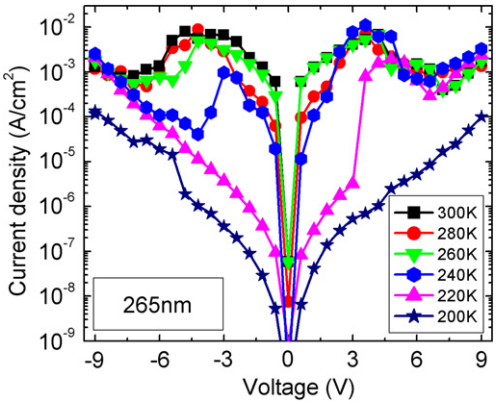

Figure 7. Absolute value of current density (J) as a function of voltage (V) plot, representing the current density level in NDR at different temperature (K).

We have also performed temperature dependent studies of the NDR in a 5 wt% PCBM:PS device as shown in figure 7. We found the maximum current density was unchanged down to 240 K, consistent with tunneling. However, below 200 K the NDR disappeared and the current density level decreases orders of magnitude very quickly.

We note that the NDR-type temperature independent I–V characteristics together with the thickness and concentration dependent current density values, all points towards tunneling. However, we then would also require thickness dependent V_{max} and V_{min}, which has not been observed in this work. This discrepancy is not clear to us, and further work is required to clarify this issue.

4. Conclusions

We have demonstrated memory effects in the fullerene-derivative PCBM blended in an inert PS matrix and its dependence on the thickness of the active intermediate layer and concentration of the PCBM molecules. PCBM:PS devices showed NDR within a particular range of thickness for a certain weight concentration of PCBM. The morphologies of PCBM:PS thin films were studied to understand the true physical nature of the phenomenon. PCBM:PS films have shown well controlled morphology without forming any aggregates in them. Unintentional inclusion of Al into the active PCBM:PS layer and its possibility of explaining the observed NDR could be excluded based on the PCBM-concentration dependent electrical measurements and quantitative elemental analysis from the device cross-sections. From our experimental results, the parameters such as V_{th}, V_{max} and V_{min} in all devices for a certain thickness between 200 and 350 nm remained constant. We have clarified the thickness and concentration dependence of the maximum current density of these PCBM:PS devices at V_{max} and V_{min} and it is observed to be above 10. The maximum current density (J_{max}) is directly proportional to the PCBM concentration (or to the calculated inter-molecular distance between two PCBM molecules), suggesting tunneling as a probable explanation for the effect. This is also confirmed by the temperature independent NDR in these devices.

Acknowledgments

We are grateful to Dr Kjell-Mikael Källman for help with atomic force microscopy measurements and for valuable discussions with Fredrik Jansson, Dr Henrik Sandberg and Marja Vilkman. Funding for this research work has been partly provided by TEKES through the FinNano program, Academy of Finland Project no. 107684 and the Magnus Ehrnrooth foundation.

Note added in proof. In a recent article the authors have reported that the abrupt increase in the current in similar devices has been attributed to the thin metal oxide layer formed at the bottom aluminum electrode [28]. We note in figure 2 that there is a presence of small amounts of oxygen at the Al/PCBM:PS interface which can be due to the presence of a native Al_2O_3 layer. This can give rise to the threshold voltage (V_{th}) shown in figure 1. This also supports the thickness independence of V_{th} shown in figure 4.

References

[1] Scott J C and Bozano L D 2007 Nonvolatile memory elements based on organic materials *Adv. Mater.* **19** 1452–63
[2] Yang Y, Ouyang J, Ma L, Tseng R J-H and Chu C-W 2006 Electrical switching and bistability in organic/polymer thin films and memory devices *Adv. Funct. Mater.* **16** 1001–14
[3] Tondelier D, Lmimouni K, Vuillaume D, Fery C and Haas G 2004 Metal/organic/metal bistable memory devices *Appl. Phys. Lett.* **85** 5763–5
[4] Ouisse T and Stéphan O 2004 Electrical bistability of polyfluorene devices *Org. Electron.* **5** 251–6
[5] Majumdar H S, Bandyopadhyay A, Bolognesi A and Pal A J 2002 Memory device applications of a conjugated polymer: role of space charge *J. Appl. Phys.* **91** 2433–7
[6] Majumdar H S, Baral J K, Österbacka R, Ikkala O and Stubb H 2005 Fullerene-based bistable devices and associated negative differential resistance effect *Org. Electron.* **6** 188–92
[7] Paul S, Kanwal A and Chhowalla M 2006 Memory effect in thin films of insulating polymer and C_{60} nanocomposites *Nanotechnology* **17** 145–51
[8] Jakobsson F L E, Crispin X and Berggren M 2005 Towards addressable organic impedance switch devices *Appl. Phys. Lett.* **87** 063503–5
[9] Nakasha Y and Watanabe Y 1995 Resonance tunnel diode memory *US Patent Specification* 5390145
[10] Cölle M, Büchel M and de Leeuw D M 2006 Switching and filamentary conduction in non-volatile organic memories *Org. Electron.* **7** 305–12
[11] Efimenko K, Rybka V, Švorčík V and Hnatowicz V 1998 Electrical properties of Au-polystyrene-Au submicron structures *Appl. Phys.* A **67** 503–5
[12] Tang W, Shi H, Xu G, Ong B S, Popovic Z D, Deng J, Zhao J and Rao G 2005 Memory effect and negative differential resistance by electrode-induced two-dimensional single-electron tunneling in molecular and organic electronic devices *Adv. Mater.* **17** 2307–11
[13] Rozenberg M J, Inoue I H and Sanchez M J 2006 Strong electron correlation effects in nonvolatile electronic memory devices *Appl. Phys. Lett.* **88** 033510–2
[14] Verbakel F, Meskers S C J and Janssen R A J 2006 Electronic memory effects in diodes from a zinc oxide nanoparticle–polystyrene hybrid material *Appl. Phys. Lett.* **89** 102103
[15] Prakash A, Ouyang J, Lin J-L and Yang Y 2006 Polymer memory device based on conjugate polymer and gold nanoparticles *J. Appl. Phys.* **100** 054309–13

[16] Juška G, Arlauskas K, Viliunas M, Genevičius K, Österbacka R and Stubb H 2000 Charge transport in π-conjugated polymers from extraction current transients *Phys. Rev.* B **62** R16235
[17] Thurstans R E and Oxley D P 2002 The electroformed metal–insulator–metal structure: a comprehensive model *J. Phys. D: Appl. Phys.* **35** 802–9
[18] Aneja A and Wilkes G L 2003 A systematic series of 'model' PTMO based segmented polyurethanes reinvestigated using atomic force microscopy *Polymer* **44** 7221–8
[19] Bulle-Lieuwma C W T, van Gennip W J H, van Duren J K J, Jonkheijm P, Janssen R A J and Niemantsverdriet J W 2003 Characterization of polymer solar cells by TOF-SIMS depth profiling *Appl. Surf. Sci.* **203/204** 547–50
[20] Savenije T J, Kroeze J E, Wienk M M, Kroon J M and Warman J M 2004 Mobility and decay kinetics of charge carriers in photoexcited PCBM/PPV blends *Phys. Rev.* B **69** 155205
[21] Bobbert P A *et al* 2007 private communication
[22] Anil Kumar C R, Deepa S, Mishra A K and Sarathi R 2003 Investing into the failure of XLPE cables due to electrical treeing: a physico chemical approach *Polym. Test.* **22** 313–8
[23] Li F, Son D-I, Cha H-M, Seo S-M, Kim B-J, Kim H-J, Jung J-H and Kim T W 2007 Memory effects of CdSe/ZnS nanoparticles embedded in a conducting poly[2-methoxy-5-(2-ethylhexyloxy)-1,4-phenylene-vinylene] polymer layer *Appl. Phys. Lett.* **90** 222109–11
[24] Kiesow A, Morris J E, Radehaus C and Heilmann A 2003 Switching behavior of plasma polymer films containing silver nanoparticles *J. Appl. Phys.* **94** 6988–90
[25] Rozenberg M J, Inoue I H and Sánchez M J 2004 Nonvolatile memory with multilevel switching: a basic model *Phys. Rev. Lett.* **92** 178302–5
[26] Shklovskii B I and Efros A L 1984 *Electronic Properties of Doped Semiconductors* (Berlin: Springer)
[27] Arkhipov V I, Fishchuk I I, Kadashchuk A and Bässler H 2006 Charge transport in disordered organic semiconductors *Photophysics of Molecular Materials* ed G Lanzani (Mannheim: Wiley)
[28] Verbakel F, Meskers S C J, Janssen R A J, Gomes H L, Cölle M, Büchel M and de Leeuw D M 2007 Reproducible resistive switching in nonvolatile organic memories *Appl. Phys. Lett.* **91** 192103